Proceedings Paper:

Generation of strongly-coupled plasma using Argon-based capillary discharge lasers

Andrew K. Rossall[*a], Valentin Aslanyan[a], Sarah Wilson[a], Greg J. Tallents[*a]

[a]York Plasma Institute, University of York, Heslington, York, YO10 5DD, United Kingdom

ABSTRACT

Argon based capillary discharge lasers operate in the extreme ultra violet (EUV) at 46.9 nm with an output of up to 0.5 mJ energy per pulse and up to a 10 Hz repetition rate. Focussed irradiances of up to 10^{12} W cm^{-2} are achievable and can be used to generate plasma in the warm dense matter regime by irradiating solid material. To model the interaction between such an EUV laser and solid material, the 2D radiative-hydrodynamic code POLLUX has been modified to include absorption via direct photo-ionisation, a super-configuration model to describe the ionisation dependant electronic configurations and a calculation of plasma refractive indices for ray tracing of the incident EUV laser radiation. A simulation study is presented, demonstrating how capillary discharge lasers of 1.2ns pulse duration can be used to generate strongly coupled plasma at close to solid density with temperatures of a few eV and energy densities up to 1×10^5 J cm^{-3}. Plasmas produced by EUV laser irradiation are shown to be useful for examining the equation-of-state properties of warm dense matter. One difficulty with this technique is the reduction of the strong temperature and density gradients which are produced during the interaction. Methods to inhibit and control these gradients will be examined.

Keywords: High energy density physics, EUV lasers, x-ray lasers, warm dense matter, strongly-coupled plasma, laser ablation

1. INTRODUCTION

Strongly coupled plasmas exist widely in the known universe. Such examples include Jovian planets, stellar interiors, laser heating of solids and capillary discharges to name a few. A strongly coupled plasma is such that the potential energy caused by the Coulombic interaction between the particles exceeds the kinetic energy of the particles. As a result, inter-particle interactions strongly affect the behaviour of individual particles, resulting in a regime which can no longer be treated as a screened Coulomb system such as a lower density or 'ideal' plasma. The strength of the coupling in a plasma is defined using the ion-ion Coulomb coupling parameter (Γ_{ii}) defined as

$$\Gamma_{ii} = \frac{Z^2 e^2}{4\pi\epsilon_0 a k T_i} \quad (1)$$

where Z is the ion charge, T_i is the ion temperature and a is the Wigner-Seitz radius which defines the inter-particle spacing. A plasma with a coupling parameter of $\Gamma_{ii} \gg 1$ is strongly coupled, $\Gamma_{ii} \approx 1$ is typically in the warm dense matter regime and $\Gamma_{ii} \ll 1$ is weakly coupled, i.e. behaves as a classical plasma.

Generation of strongly coupled plasma in the laboratory using laser irradiation as a heating source has typically involved irradiating buried layer targets[1] to inhibit expansion of the target material. With advances in capillary discharge laser technology[2–5] and an associated increase in fluence available, argon based capillary discharge lasers operating at 46.9nm can be used to directly generate strongly coupled plasma on a picosecond time-scale with simple single-layer planar targets. In reducing the photon wavelength to the extreme ultra-violet (EUV), the dominant heating mechanism changes from inverse bremsstrahlung to direct photo-ionisation and the critical electron density at this wavelength is typically higher than solid. The sub-critical electron density combined with a short penetration depth (<100nm in parylene-N at 26.4eV) and a smaller focal spot size due to the reduction in the diffraction limit improves the localisation of energy deposition within the target. A

*Further author information:
E-mail: andrew.rossall@york.ac.uk, Telephone: +44 (0)1904 324909
E-mail: greg.tallents@york.ac.uk, Telephone: +44 (0)1904 322286

small volume is heated (approximately $5 \times 10^{-4} \mu\text{m}^3$ in parylene-N for a FWHM beam diameter of 500nm) until photo-ionisation is no longer energetically possible at which point the volume becomes mostly transparent to the incident EUV laser beam. It is worth noting that inverse bremsstrahlung can become non-negligible in regions where the electron density is within an order of magnitude of the critical electron density.

The simulation study presented here utilises a combination of 2D hydrodynamic modelling with an atomic physics algorithm to demonstrate how capillary discharge lasers of 1.2ns pulse duration with pulse energies up to 0.8mJ can be used to generate strongly coupled plasma at close to solid density with temperatures of a few eV and energy densities up to $\sim 10^6$ J cm^{-3}.

2. POLLUX

2.1 General Overview

The 2D Eulerian radiative-hydrodynamic code POLLUX,[6,7] written at the University of York, was originally developed to model moderate irradiance ($\geq 10^{10}$ W cm^{-2}) optical and infra-red laser irradiation of a solid target and the subsequently produced strongly ionised plasma. This code has been modified to include a rapid atomic physics algorithm,[8,9] to enable the calculation of ionisation and energy level populations and atomic scattering factors in the EUV for partially ionised plasmas. The algorithm for the code is shown in figure 1. The code solves the three first-order quasi-linear partial differential equations of hydrodynamic flow using the flux corrected transport model of Boris and Book[10] with an upwind algorithm[11] for the first term. Energy is absorbed by the plasma electrons through inverse bremsstrahlung and direct photo-ionization and distributed through electron-ion collisions. The electron-ion equilibration rate is determined by the Spitzer plasma collision rate[12] and is limited to the electron-phonon collision frequency in the low temperature regime (< 5eV). For calculation of the equation-of-state (EOS) variables, POLLUX utilizes in-line hydrodynamic EOS subroutines from the Chart-D[13] equation-of-state package developed st Sandia National Laboratories and includes two-phase transitions. As this code uses an explicit solver, a Courant number of ~ 1 in both spatial directions increases numerical stability. We have for the Courant number,

$$C = \frac{u_x \Delta t}{\Delta x} + \frac{u_y \Delta t}{\Delta y} \approx 1 \tag{2}$$

where u_x and u_y are magnitudes of the particle velocities in the respective directions, Δt is the time step and $\Delta x, \Delta y$ are the cell spatial dimensions. This is not the only constraint on the simulation parameters, however it is the most restrictive.

2.2 Atomic Physics Algorithm

A superconfiguration approach[15] allows for multiple electronic configurations that are close in energy to be grouped together, significantly reducing the number of levels to be considered. The average energy $\langle E \rangle_{SS}$ of m levels each with energy E_m is weighted by the degeneracy, g_m. Detailed atomic structure is calculated using the flexible atomic code (FAC) to solve the radial wave equation, this structure is then post-processed using the relationship shown in equation 3 to form a reduced set of configurations.

$$\langle E \rangle_{SS} = \frac{\sum_m g_m E_m}{\sum_m g_m}, \tag{3}$$

Ionisation and level populations are calculated assuming local thermodynamic equilibrium, an assumption which has been justified for hydrodynamic time scales (> 1 ps), as the equilibration of the plasma occurs on a timescale of 10s of femtoseconds.[16] Photoionisation cross-sections are calculated assuming an E^{-3} dependence, the atomic scattering factor, $f_1^0(E)$, is then calculated using an analytical solution to the Kramers-Kronig relationship as reported previously.[9] The real component of the plasma refractive index can then be calculated. In a dense plasma, the threshold ionization energy can be significantly lowered due to the presence of surrounding free electrons and ions. The time averaged effects of the ionisation potential depression is accounted for in the code using the Stewart-Pyatt model.[17,18]
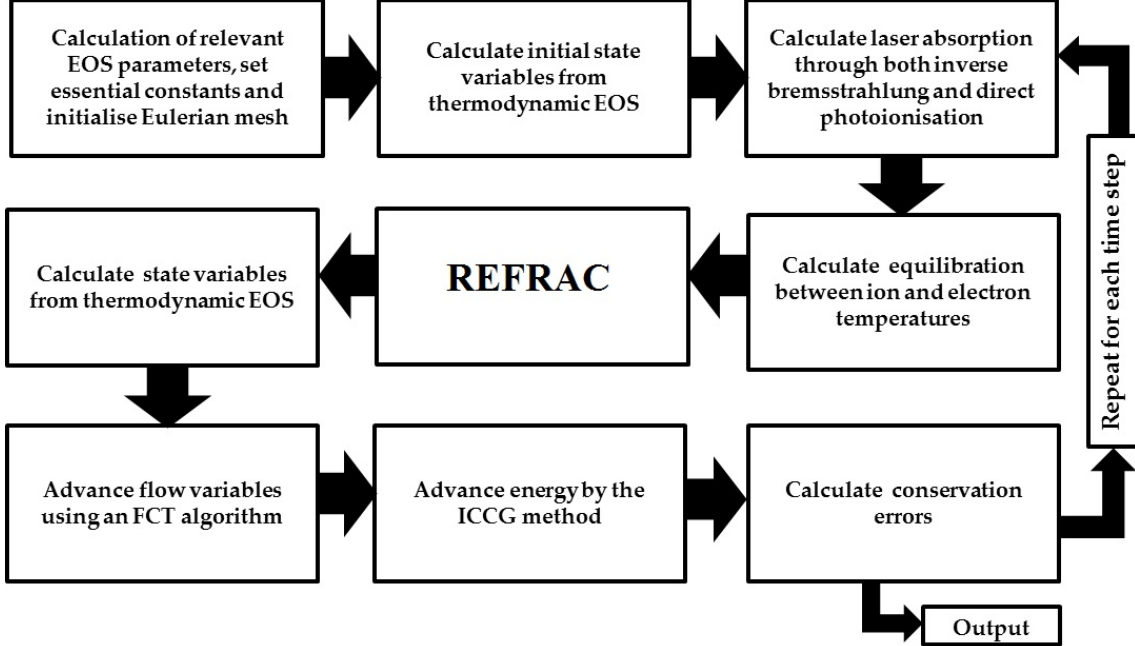
Figure 1. Complete POLLUX algorithm using the flux corrected transport (FCT) algorithm,[10] the incomplete Cholesky-conjungate gradient (ICCG) method[14] and the REFRAC module, outlined in section
.

To enable ray tracing of the incident EUV laser pulse within the code, the Eulerian mesh is sub-divided into triangular cells with the Eulerian mesh center points at the triangle corners allowing for the refractive index and associated gradient within each cell to be calculated via direct differencing. The refractive index is continuous across cell boundaries and assumes a linear electron density variation within each cell. The (x, y) trajectory of each ray in the cell is then assumed to be parabolic dependent upon the refractive index n_0 and its derivative n_1, given by,

$$y^2 = 4\left(\frac{n_0}{n_1}\right)x. \tag{4}$$

3. RESULTS AND DISCUSSION

To determine the potential of capillary discharge lasers for the generation of strongly coupled plasma, the EUV laser-solid interaction is simulated for irradiances of 1×10^{10} W cm^{-2} and 1×10^{14} W cm^{-2} incident on parylene-N and aluminium planar targets. The simulation environment is cylindrically symmetric (Z, r) with the laser propagating from positive to negative Z along $r = 0$, with the solid target in the region $Z < 0$. The linear density ramp for the target surface begins at $Z = 0$ and covers 2 cells in the Z direction.

Figures 2 and 3 show particle densities (n), electron temperatures (T_e) and energy densities for parylene-N and aluminium for irradiances of 10^{10} and 10^{14} W cm^{-2}. For the lowest irradiance, electron temperatures of 8 to 10 eV are calculated for both parylene-n and aluminium with energy densities up to 9×10^4 J cm^{-3}. With particle densities of $\sim 10^{22}$ cm^{-3} in the hottest region, both parylene-N and aluminium are in a warm dense matter regime. Increasing the irradiance of the EUV laser to 10^{14} W cm^{-2} produces a plasma in the high energy density regime ($> 10^5$ J cm^{-3}). Energy densities up to 9×10^5 J cm^{-3} are calculated for the aluminium plasma, with the high energy density region having a depth of ~ 500nm at the earliest simulation time of 100ps. These narrow peaks in energy density are due to the short absorption length of 26.4 eV photons and emission from this region will not be masked by a hotter, less dense plasma plume as is often observed with optical and infra-red laser interactions.
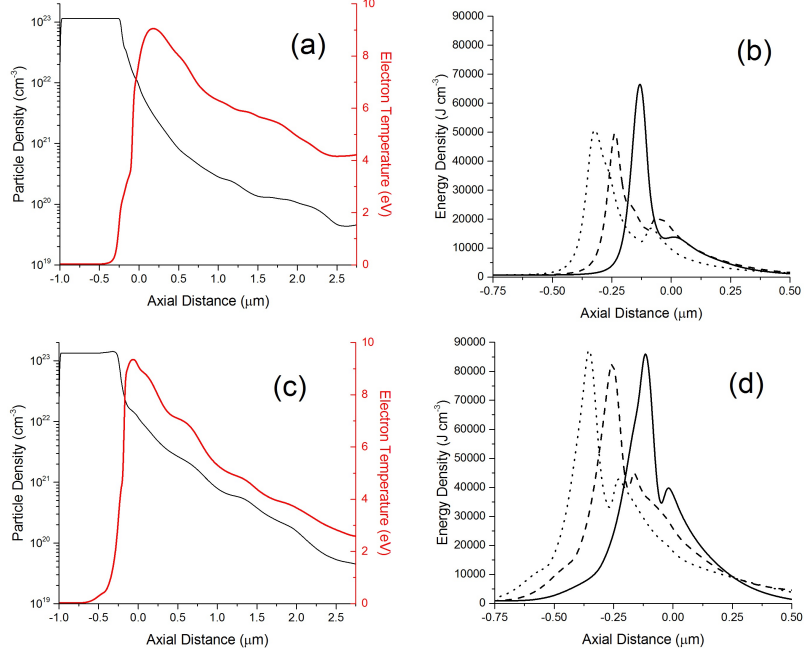
3

Figure 2. Particle density, electron temperature and energy density as a function of axial distance (distance along laser axis) for parylene-N ((a) and (b))and aluminium ((c) and (d)). For (a) and (c) the simulation time is $t = 200$ps and for (b) and (d) the simulation times are $t = 100$ps (solid line), $t = 200$ps (dashed line), and $t = 300$ps (dotted line). The on target irradiance is 10^{10} W cm^{-2}.
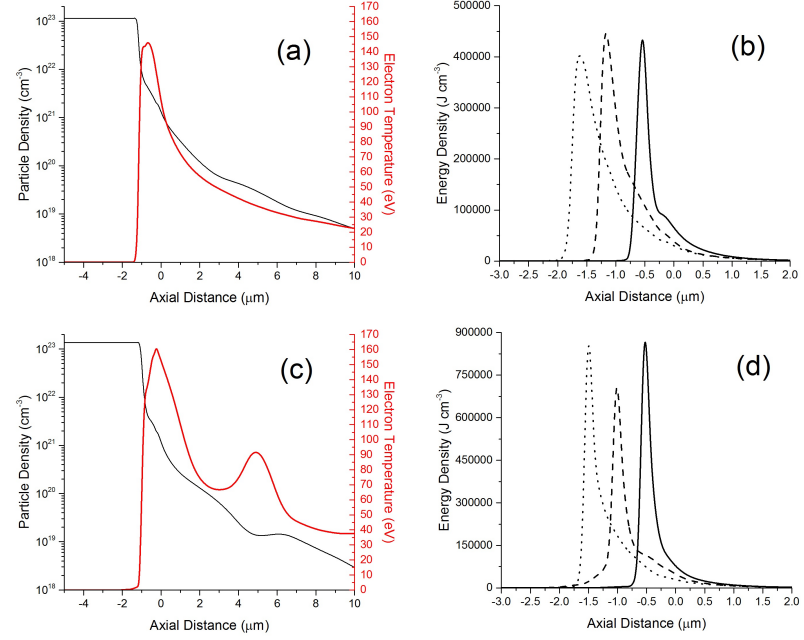

Figure 3. Particle density, electron temperature and energy density as a function of axial distance for parylene-N ((a) and (b))and aluminium ((c) and (d)). For (a) and (c) the simulation time is $t = 200$ps and for (b) and (d) the simulation times are $t = 100$ps (solid line), $t = 200$ps (dashed line), and $t = 300$ps (dotted line). The on target irradiance is 10^{14} W cm^{-2}.
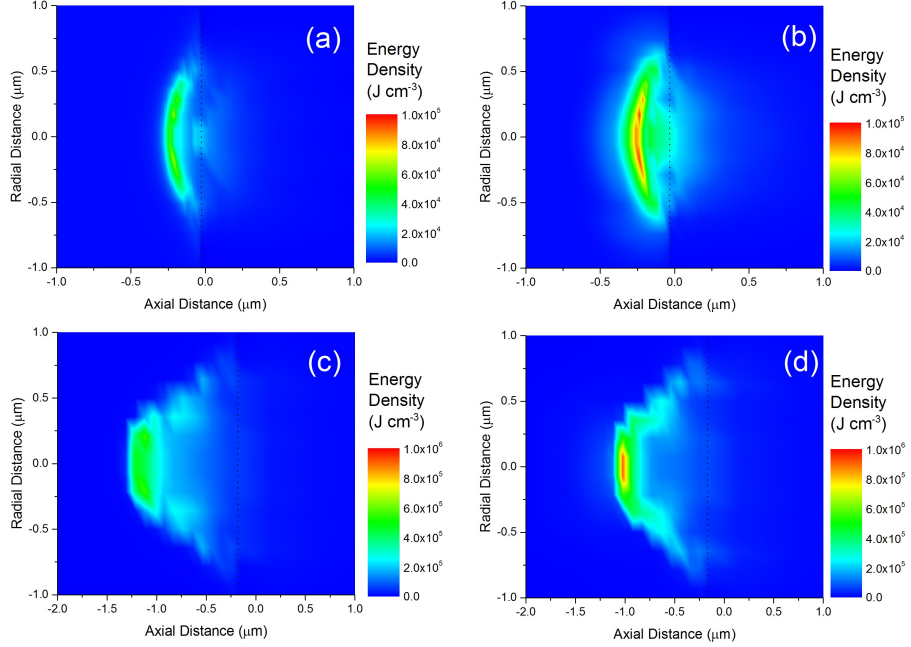
4

Figure 4. Two-dimensional energy density plots for parylene-N with on-target irradiance of (a) 10^{10}W cm^{-2} and (b)10^{14}W cm^{-2}, and aluminium with on-target irradiance of (c) 10^{10}W cm^{-2} and (d) 10^{14}W cm^{-2}

.

Figure 4 shows 2 dimensional plots of energy density for both parylene-N and aluminium. Small volumes of dense plasma are effectively heated where the volume of the high energy density region appears to decrease with increasing laser irradiance. Coupling parameters of up to $\Gamma_{ii} \approx 45$ can be observed in aluminium and up to $\Gamma_{ii} \approx 18$ in parylene-N as shown in figure 5. Due to emission having an n^2 dependence, emission from these regions will dominate over the hotter less dense expanding plasma. The temperature and particle densities of the high energy density regions remain approximately constant for ~ 300ps, therefore a sufficiently fast camera or streak camera would be able to temporally resolve the emission from these regions.
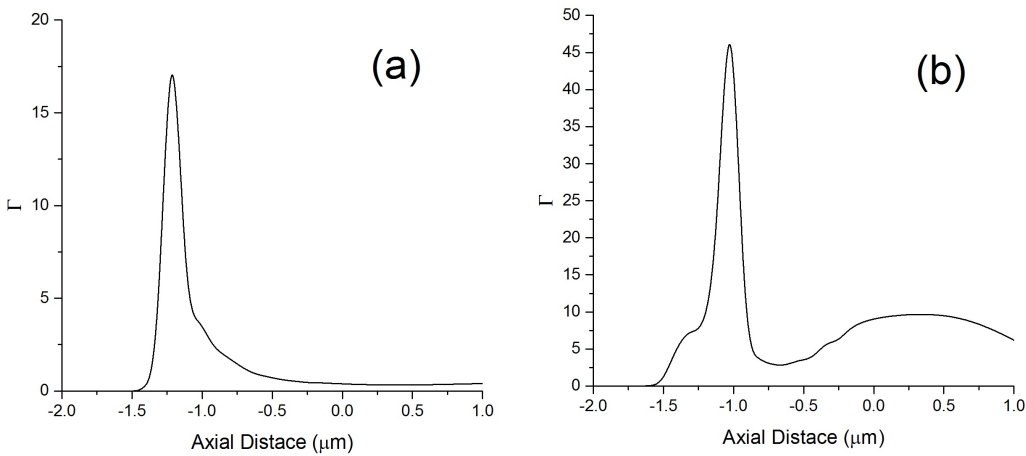

Figure 5. Coupling parameter as a function of axial distance for (a) parylene-N and (b) aluminium, on target irradiance is 10^{14} W cm^{-2}

.

When studying equation-of-state (EOS) parameters, perfect volumetric heating of the target would be ideal to ensure uniform heat flow within the target. Temperature and density gradients arising from non-uniformities associated with heat flow make simulations and/or analysis of experiments investigating warm or hot dense matter difficult. Using a capillary discharge laser to generate warm and hot dense plasma simplifies the problem as a linear approximation for the temperature and density gradients would be suitable for EOS and opacity modelling as done previously.[19]

4. CONCLUSIONS

The 2-dimensional hydrodynamic code POLLUX has been modified to include atomic physics processes relevant to the interaction of EUV photons with solid matter. Through this simulation study, it has been shown that capillary discharge lasers operating at 26.4eV can be used to generate warm and hot dense matter with a coupling parameter as high as $\Gamma_{ii} \approx 50$ and energy density of 9×10^9 J cm^{-3} in aluminium. This technique is shown to be useful for examining the properties of strongly coupled plasma as emission from this region is not masked by the hotter less dense expanding plasma as with optical and infra-red interactions. Linear approximations for temperature and density gradients are shown to be suitable to simplify the simulation and/or analysis of experiments investigating equation-of-state parameters or plasma opacity.

REFERENCES

[1] Gregori, G., Hansen, S. B., Clarke, R., Heathcote, R., Key, M. H., King, J., Klein, R. I., Izumi, N., Mackinnon, A. J., Moon, S. J., Park, H.-S., Pasley, J., Patel, N., Patel, P. K., Remington, B. A., Ryutov, D. D., Shepherd, R., Snavely, R. A., Wilks, S. C., Zhang, B. B., and Glenzer, S. H., "Experimental Characterization of a Strongly Coupled Solid Density Plasma Generated in a Short-pulse Laser Target Interaction," *Contributions to Plasma Physics* **45**(3-4), 284–292 (2005).

[2] Rocca, J. J., Hammarsten, E. C., Jankowska, E., Filevich, J., Marconi, M. C., Moon, S., and Shlyaptsev, V. N., "Application of extremely compact capillary discharge soft x-ray lasers to dense plasma diagnostics," *Physics of Plasmas* **10**(5), 2031 (2003).

[3] Benware, B., Macchietto, C., Moreno, C., and Rocca, J., "Demonstration of a High Average Power Tabletop Soft X-Ray Laser," *Physical Review Letters* **81**(26), 5804–5807 (1998).

[4] Heinbuch, S., Grisham, M., Martz, D., and Rocca, J. J., "Demonstration of a desk-top size high repetition rate soft x-ray laser," *Optics Express* **13**(11), 4050 (2005).

[5] Macchietto, C. D., Benware, B. R., and Rocca, J. J., "Generation of millijoule-level soft-x-ray laser pulses at a 4-Hz repetition rate in a highly saturated tabletop capillary discharge amplifier," *Optics Letters* **24**(16), 1115 (1999).

[6] Pert, G. J., "Two-dimensional hydrodynamic models of laser-produced plasmas," *Journal of Plasma Physics* **41**(02), 263–280 (1989).

[7] Pert, G., "Quasi-Lagrangian rezoning of fluid codes maintaining an orthogonal mesh," *Journal of Computational Physics* **49**(1), 1–43 (1983).

[8] Rossall, A. K., Aslanyan, V., Tallents, G. J., Kuznetsov, I., Rocca, J. J., and Menoni, C. S., "Ablation of Submicrometer Holes Using an Extreme-Ultraviolet Laser," *Physical Review Applied* **3**(6), 064013 (2015).

[9] Rossall, A. K. and Tallents, G. J., "Generation of Warm Dense Matter using an Argon based Capillary Discharge Laser," *High Energy Density Physics* **15** (2015).

[10] Boris, J. and Book, D., "Flux-corrected transport. III. Minimal-error FCT algorithms," *Journal of Computational Physics* **20**(4), 397–431 (1976).

[11] Courant, R., Isaacson, E., and Rees, M., "On the solution of nonlinear hyperbolic differential equations by finite differences," *Communications on Pure and Applied Mathematics* **5**(3), 243–255 (1952).

[12] Spitzer, L. and Härm, R., "Transport Phenomena in a Completely Ionized Gas," *Physical Review* **89**(5), 977–981 (1953).

[13] Thompson, S. L., "Improvements in the CHART-D radiation-hydrodynamic code I: Analytical equation of state," *Sandia National Laboratories Report* **SC-RR-70-2** (1970).

[14] Kershaw, D. S., "The incomplete Choleskyconjugate gradient method for the iterative solution of systems of linear equations," *Journal of Computational Physics* **26**(1), 43–65 (1978).

[15] Hansen, S. B., Bauche, J., and Bauche-Arnoult, C., "Superconfiguration widths and their effects on atomic models," *High Energy Density Physics* **7**(1), 27–37 (2011).

[16] Aslanyan, V. and Tallents, G. J., "Local thermodynamic equilibrium in rapidly heated high energy density plasmas," *Physics of Plasmas* **21**(6), 062702 (2014).

[17] Stewart, J. C. and Pyatt, K. D., "Lowering of Ionization Potentials in Plasmas," *The Astrophysical Journal* **144**, 1203 (1966).

[18] Preston, T. R., Vinko, S. M., Ciricosta, O., Chung, H.-K., Lee, R. W., and Wark, J. S., "The effects of ionization potential depression on the spectra emitted by hot dense aluminium plasmas," *High Energy Density Physics* **9**(2), 258–263 (2013).

[19] Nagayama, T., Bailey, J. E., Rochau, G. A., Hansen, S. B., Mancini, R. C., MacFarlane, J. J., and Golovkin, I., "Investigation of iron opacity experiment plasma gradients with synthetic data analyses.," *The Review of scientific instruments* **83**, 10E128 (Oct. 2012).